Biomech Model Mechanobiol (2011) 10:339–355
DOI 10.1007/s10237-010-0238-2

ORIGINAL PAPER

Mechanistic insight into the physiological relevance of helical blood flow in the human aorta: an in vivo study

Umberto Morbiducci · Raffaele Ponzini · Giovanna Rizzo · Marcello Cadioli · Antonio Esposito · Franco Maria Montevecchi · Alberto Redaelli

Received: 22 December 2009 / Accepted: 30 June 2010 / Published online: 22 July 2010

Abstract The hemodynamics within the aorta of five healthy humans were investigated to gain insight into the complex helical flow patterns that arise from the existence of asymmetries in the aortic region. The adopted approach is aimed at (1) overcoming the relative paucity of quantitative data regarding helical blood flow dynamics in the human aorta and (2) identifying common characteristics in physiological aortic flow topology, in terms of its helical content. Four-dimensional phase-contrast magnetic resonance imaging (4D PC MRI) was combined with algorithms for the calculation of advanced fluid dynamics in this study. These algorithms allowed us to obtain a 4D representation of intra-aortic flow fields and to quantify the aortic helical flow. For our purposes, helicity was used as a measure of the alignment of the velocity and the vorticity. There were two key findings of our study: (1) intra-individual analysis revealed a statistically significant difference in the helical content at different phases of systole and (2) group analysis suggested that aortic helical blood flow dynamics is an emerging behavior that is common to normal individuals. Our results also suggest that helical flow might be caused by natural optimization of fluid transport processes in the cardiovascular system, aimed at obtaining efficient perfusion. The approach here applied to assess in vivo helical blood flow could be the starting point to elucidate the role played by helicity in the generation and decay of rotating flows in the thoracic aorta.

Keywords 4D phase-contrast MRI · Perfusion · Spiral flow · Fluid mechanics · Aortic arch · Hemodynamics

Electronic supplementary material The online version of this article (doi:10.1007/s10237-010-0238-2) contains supplementary material, which is available to authorized users.

U. Morbiducci (✉) · F. M. Montevecchi
Department of Mechanics, Politecnico di Torino,
Corso Duca degli Abruzzi, 24, 10129 Turin, Italy
e-mail: umberto.morbiducci@polito.it

R. Ponzini
CILEA, Interuniversity Consortium, Milan, Italy

G. Rizzo
Istituto di Bioimmagini e Fisiologia Molecolare,
Research National Council, Milan, Italy

M. Cadioli
Philips Medical Systems, Milan, Italy

A. Esposito
Department of Radiology, Scientific Institute H S Raffaele,
Milan, Italy

A. Redaelli
Department of Bioengineering, Politecnico di Milano,
Milan, Italy

1 Introduction

The human aorta is the major vessel that transports blood pumped by the left ventricle to the systemic circulation. The complex hemodynamics that are observed in the human aorta partially originate in the complicated geometry, including (1) the non-planar curvatures (Yearwood and Chandran 1982; Chandran 1993), (2) the branches at the apex of the arch, (3) the significant tapering of distensible vessel walls, (4) the dynamic movements of the ascending aorta, (5) the structures projecting into the flowing blood stream at or above the aortic valve (Bellhouse and Talbot 1969), and (6) the ventricular twisting and torsion during contraction (Baciewicz et al. 1991). The other reason for the observed complexity is that the thoracic aorta is the site in the healthy cardiovascular system where laminar-turbulent transitional flows are present.

All of these reasons could strongly elicit the onset of helical patterns in aortic blood flow, which are assumed to facilitate ventricular ejection even if their relation to physiology is still unclear (Stonebridge et al. 1996). This conjecture as to the role played by helical flow in the aorta is consistent with the fundamental role recognized for helicity, a measure of the alignment of velocity and vorticity, (1) in the organization of both laminar and turbulent flow topologies (Moffatt 1969, 1990) and (2) in the arrest of the energy decay (Moffatt and Tsinober 1992).

Because blood flow in the aorta is intricate, massive in vivo measurement campaigns have been performed in the past (Seed and Wood 1971; Segadal and Matre 1987; Kilner et al. 1993; Morbiducci et al. 2009a) that demonstrated that helical flow is predominant in areas from the ascending aorta to the aortic arch. This form of blood flow is also a basic pattern for almost all of the subjects, regardless of age and gender (Bogren and Buonocore 1999; Buonocore and Bogren 1999; Houston et al. 2003). In the last decades, the PC MRI technique has become the prevalent imaging technique for non-invasive and detailed quantification of blood flow. Other than its non-invasive procedure, the main reason that PC MRI is an innovative in vivo technique is its good spatial resolution with respect to hemodynamic quantities. Additionally, this technique allows for the possibility of acquiring time-dependent data sets that are necessary to perform reliable and local hemodynamic characterization. Due to its features, PC MRI has provided insight into the hemodynamics of the aorta in animal models (e.g., Amirbekian et al. 2009) and in humans (Kilner et al. 1993; Bogren and Buonocore 1999; Markl et al. 2004; Hope et al. 2007; Morbiducci et al. 2009a), where it has been used to illustrate clinical aortic physiopathological findings (for example Markl et al. 2004; Frydrychowicz et al. 2007). However, flow patterns may be overlooked if only visualization tools are used. All of the in vivo observations of aortic flow topologies associated with common physiological and pathological findings that are available in the literature are based on qualitative visual evaluation; the mechanistic role that these emerging flow features play in aorta hemodynamics remains unclear. Recently, to answer questions regarding the nature and origins of complex flow patterns in the human aorta, we investigated the distribution of helical blood flow in the aortic arch with 4D PC MRI data (Morbiducci et al. 2009a). In detail, we obtained the complete spatio-temporal description of blood flow in the aorta employing time-resolved PC MRI.

In this paper, we present the results of in vivo helical flow quantification in the aortas of five healthy humans, performed employing 4D PC MRI. Our study is aimed at identifying common characteristics in healthy aortic flow topology in terms of its helical content. Technically, the method proposed by the authors in 2009 (Morbiducci et al. 2009a) was applied to the data from healthy volunteers, making use of tools developed for computational fluid dynamics. In particular, we mapped the patterns of the transient flow in the human aortic arch in detail and quantified helical structures. This quantitative approach allowed us to rank the behavior of flowing blood and identify emerging physiological flow features. A method for helical flow quantification, which has been developed to reveal the global organization of blood flow, was applied to the datasets (Grigioni et al. 2005; Morbiducci et al. 2007a; Morbiducci et al. 2007b; Morbiducci et al. 2009a).

The results of this study could help elucidate the role played by helicity in the generation and decay of rotating flows in the thoracic aorta.

2 Materials and methods

2.1 Theoretical remarks on helicity

In fluid mechanics, mathematical concepts have been borrowed from knot theory, graph theory, dynamical systems theory, and other branches of modern mathematics. These concepts can be usefully employed in the analysis of flows to quantify, estimate, or infer production, transfer, and depletion of physical quantities such as energy and momentum (Moffatt 1990; Ricca 2009). The origin of topological fluid mechanics is most likely rooted in the studies of vortex motion by Helmholtz in 1858 and Kelvin in 1869. Much of its modern developments are due to recent progress in vector field analysis, mathematical fluid dynamics, and computational visualization. In fact, in recent years, the demand for advanced diagnostic tools for computational and experimental bio-fluids has grown considerably. Detailed analysis of space localization and time evolution of coherent structures, defined by statistical coherence of physically relevant quantities (vector or tensor fields, scalars), requires metrics to quantify structural complexity present in flowing blood. In particular, a better understanding of the critical role of blood flow evolution through the formation and disappearance of spiral patterns can be obtained through helicity, a scalar that is eligible to study relationships between complexity and energy. Helicity can be thought of as the degree to which the velocity field lines wrap and coil around each other (Moffatt and Tsinober 1992). The physical meaning of this quantity is fundamental in relation to flow kinematics because it admits topological interpretation in relation to linkages of vortex lines of the flow.

The helicity H(t) of a fluid flow confined to a domain D of the three-dimensional Euclidean space $\mathbf{R}^3$ is the integrated internal product of the velocity field $\mathbf{V}(\mathbf{s}; t)$ and the vorticity field $\boldsymbol{\omega}(\mathbf{s}; t) = \nabla \times \mathbf{V}(\mathbf{s}; t)$:

$$H(t) = \int_D \mathbf{V}(\mathbf{s}; t) \cdot \boldsymbol{\omega}(\mathbf{s}; t)\, ds. \quad (1)$$

The pseudo-scalar quantity $H_k(\mathbf{s};t)$, given by

$$H_k(\mathbf{s};\ t) = \mathbf{V}(\mathbf{s};\ t) \cdot \boldsymbol{\omega}(\mathbf{s};\ t), \quad (2)$$

is the density per unit volume of kinetic helicity. Both H(t) and $H_k(\mathbf{s};\ t)$ are pseudo-scalars, i.e., roughly speaking they have opposite sign when they are viewed from a right-handed or a left-handed frame of reference.

The law of conservation in fluid flow of H(t) is important because this quantity organizes the flow and characterize the changes of its structure over time (Moffatt 1969). However, in a slightly viscous case such as blood flow in great vessels (Navier-Stokes flow), the extent of dissipation of the helicity or the kinetic energy is unknown (i.e., the two inviscid conserved quantities). The sole "quantitative" method to compute them exactly is simulations that make use of patient-specific models, which suffer from limitations in precisely reproducing the in vivo hemodynamics. Helicity involves higher-order spatial derivatives, namely, the smaller scales that are easier to dissipate. Equation 1 incorporates vorticity, which is given by a combination of velocity gradients. Hence, the helicity may naturally be expected to dissipate more quickly than the kinetic energy. In contrast, there is evidence that only the kinetic energy is transferred to the smaller scales. Therefore, only the kinetic energy may dissipate, while the helicity does not. Therefore, helicity, like energy, has a great influence on the evolution and stability of both laminar and turbulent flows (Moffatt and Tsinober 1992).

2.2 Data acquisition

Five healthy volunteers (men; age range 23–42 years, mean equal to 32 years (SD 9); heart rate range 43–78 bpm, mean equal to 56 bpm (SD 13) were enrolled in this study, which was conducted using a 1.5 Tesla scanner equipped with a 5-channel SENSE phased-array cardiac coil (Achieva, Philips Healthcare, The Netherlands). All volunteers underwent the entire cardiovascular magnetic resonance examination during a 60–90 min period, which included subject preparation, scanner set-up, and image data acquisition. All data were acquired during the same examination session to ensure comparability.

In vivo blood flow measurements were conducted with a three-directional phase-contrast velocity mapping sequence. The three-dimensional region of interest was set in such a way that it covered the aorta from the sinotubular region to the distal abdominal aorta. Three-dimensional data were acquired in 20–22 oblique sagittal slices (field of view = $280 \times 280\,mm^2$) aligned with the aortic arch, and the entire aorta was covered with an isotropic spatial sampling (measured voxel size: $2 \times 2\,mm^2$, with slice thickness = 4 mm, and slice spacing = 2 mm). The three components of the velocity vector field were measured by acquiring one segment with no velocity sensitivity and three segments with velocity sensitivity in each direction. The pulse sequence for 4D PC MRI data acquisition was a T1-weighted cardiac-gated respiratory-compensated 3D Phase-Contrast Turbo Gradient Echo (TR = 5.4 ms, TE = 3 ms, flip angle = 15°, velocity sensitivity = 150 cm/s) with velocity encoding along all three spatial directions.

To acquire time-resolved three-dimensional information, a phase-contrast pulse sequence had to be arranged to allow synchronization of the data to the cardiac cycle to reconstruct a cine series of three-dimensional data sets from multiple phases of the cardiac cycle. In this way, an "equivalent cardiac cycle" was obtained. Because breath holding was not possible, artifacts induced by respiratory motion were minimized using a soft band around the upper abdomen to physically restrict chest movements. A navigator-echo technique was used to further reduce motion artifacts (Firmin and Keegan 2001), with the navigator beam placed across the diaphragm and the tracking direction set to Feet-Head. The three-dimensional data were acquired in approximately 40 min or more with a navigator efficiency of 50%. Hence, for each subject, the resulting cine pulse sequence was retrospectively gated to the electrocardiographic cycle to obtain 21 cardiac phases with a temporal resolution of 38 ms.

2.3 Visualization and data analysis

User-defined tools previously developed by the authors (Morbiducci et al. 2009a; Ponzini et al. 2009) were applied to both process and analyze PC MRI data: for each subject under investigation, the dataset of the three components of the blood velocity vector field at different phases of the cardiac cycle was extracted from MRI images.

As an example of the acquired PC MRI data, Fig. 1 displays the three-directional velocity map frames (phases I, II, and III, respectively) on a plane aligned with the aortic arch, viewed from the left. In the images, brightness is proportional to signal intensity; a brighter signal corresponds to a larger positive velocity component of blood flowing into the slice. For each subject, three different phases of systole are shown.

From the three gray-scale images containing the three velocity components (Fig. 1), an additional image study that represented the velocity modulus was performed. This image study was used to generate the three-dimensional shape of the aorta. Figure 2 (upper panel) displays the three-dimensional anatomical reconstructions of the thoracic aorta of the five subjects investigated, including the branches and the measured blood flow rate waveforms (Fig. 2, lower panel). The presence of morphological differences in healthy human aortas is noteworthy. Technically, the procedure for the extraction of the aortic shape consists of two steps: (1) image segmentation by interactively drawing the aorta con-

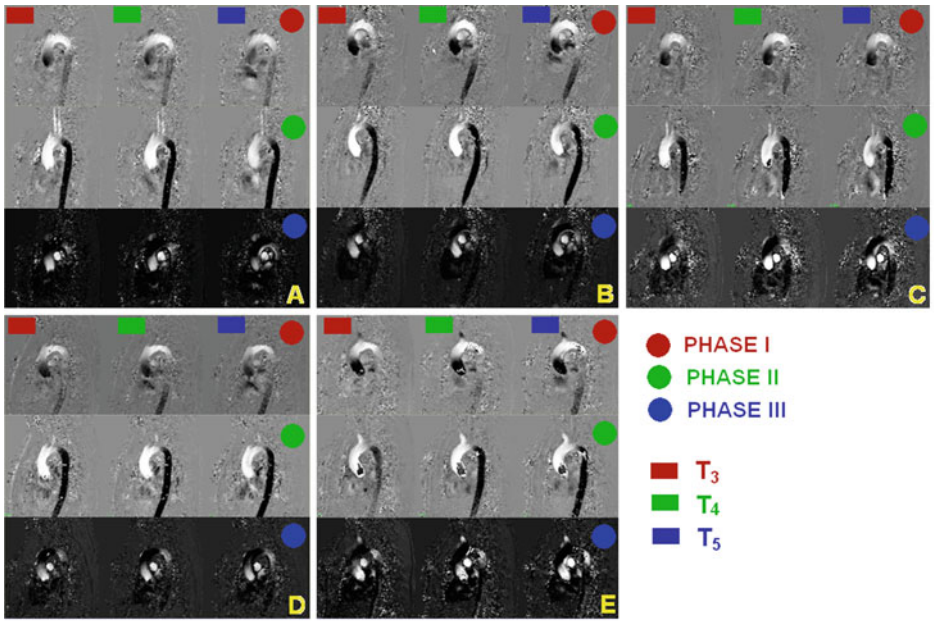

Fig. 1 Three-directional velocity map frames acquired on a plane aligned with the aortic arch, viewed from the *left*. Phases I and II are representative of the in-plane components of the velocity vector field; phase III represents the through-plane component. For each subject, nine map frames are displayed, spanning the entire systole—three phases at three different times (shown in the *lower panel*, displaying the measured blood flow rate waveforms). Brightness is proportional to signal intensity: the brighter the signal, the larger the (positive) velocity component of blood flowing into the slice

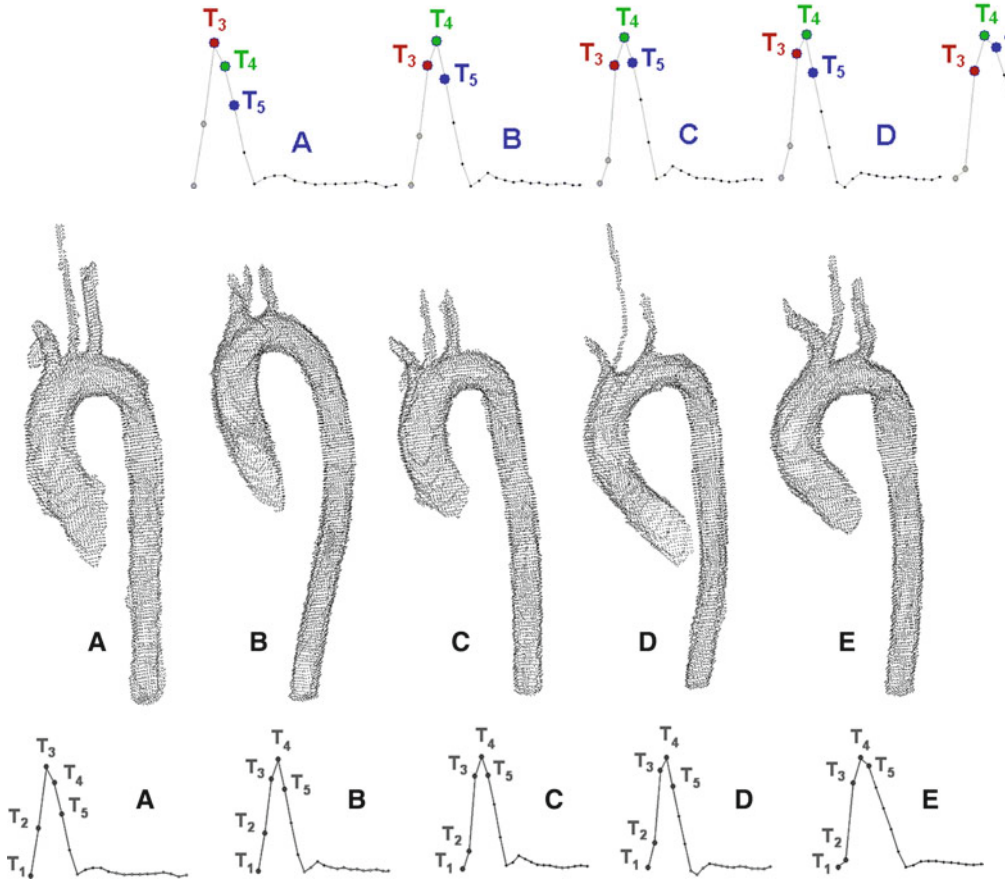

Fig. 2 The *upper panel* displays the three-dimensional shapes of the five human aortas investigated. The *lower panel* displays the measured individual blood flow rate waveforms, together with the five different time points T_j ($j = 1, \ldots, 5$) of particle set emissions, tracked in their evolution over the time interval from T_j to the end of systole

tour slice by slice using the commercial software Analyze (Biomedical Imaging Resource, Mayo Clinic, Rochester, MN) and (2) generation of the aorta surface from the segmented images by calculating the isosurface using standard built-in tools provided by Matlab 7.0 (The Mathworks, Inc, Natick, MA, USA).

We took advantage of the ability of particle traces to provide an accurate representation of unsteady features of flow fields (Steinman 2000) by performing a Lagrangian analysis of the acquired 4D PC MRI datasets. Hence, particle traces, the centerpiece of our investigation, were computed by time integration of the velocity field, starting from user-specified locations and time frames. Technically, particle trajectories were calculated in a velocity field defined by known velocities at a number of points (the measured voxels) and at certain time instants; between these points, at discrete times, velocities must be interpolated. In this study, we used the bicubic spline method, which has been shown to be accurate (David et al. 2002) for the interpolation of the velocity field both in the spatial and time domain. The particle traces were calculated using a fourth-order Runge-Kutta numerical integration scheme, which has been shown to produce an accurate particle path (Darmofal and Haimes 1996). We "released" sets of N_p immaterial particles at five different time points T_j ($j = 1, \ldots, 5$; Fig. 2, lower panel) of the measured systolic phase and tracked them (as explained above) in their evolution over the time interval from T_j to the end of systole T_{es}. To achieve this, an emitter grid was positioned in the data set to release particles at a desired time and location. No real tracer was used in this study.

The classic finite difference method was implemented for the calculation of the velocity gradients' tensor, which is needed for the calculation of the vorticity vector.

The algorithms adopted in this work for the calculation of the velocity gradients and for particle tracking, together with the bicubic spline spatio-temporal interpolation scheme, were previously validated, in order to verify their adequacy with respect to the MRI macro-parameters (Morbiducci et al. 2009a; Ponzini et al. 2009). For the visualization of vector fields and particle traces, both commercial (TECPLOT, Inc., Bellevue, WA, USA) and open source visualization tools were used to navigate through the data and analyze blood flow within the volumetric acquisition of the entire aorta.

2.4 Helical flow index as a measure of blood flow complexity

The velocity vector fields resulting from interpolation of the PC MRI measured dataset were analyzed via computation of the Lagrangian-based descriptor, the helical flow index (HFI), to obtain a "measure" of the helical structure in the blood flow. In fact, HFI has recently been demonstrated to be an effective descriptor of complex, fully three-dimensional flow fields. HFI, originally applied to computational models (Grigioni et al. 2005; Morbiducci et al. 2007a; Morbiducci et al. 2007b) and very recently tested in vivo on 4D PC MRI measurements of blood flow in the human aorta (Morbiducci et al. 2009a), calculates the content of helical motion according to a particle trace analysis of the flow.

Considering the remarks on helicity, HFI was developed to measure the helical structure of blood flow inside a vessel using the Local Normalized Helicity (LNH) as a basic quantity computed along a particle trajectory. LNH is defined as

$$\mathrm{LNH}\,(\mathbf{s};t) = \frac{\mathbf{V}\,(\mathbf{s};t)\cdot\boldsymbol{\omega}\,(\mathbf{s};t)}{|\mathbf{V}\,(\mathbf{s};t)|\,|\boldsymbol{\omega}\,(\mathbf{s};t)|} \quad -1 \leq \mathrm{LNH} \leq 1, \tag{3}$$

where $\mathbf{s}$ is the position and t is time. The non-dimensional quantity LNH is a function of space and time, and it is the local value of the cosine of the angle between the velocity and vorticity vectors. According to Eq. 3, LNH can assume values varying between one (in the module when the flow is purely helical) and zero (in the presence of fluid dynamical reflectional symmetry). Moreover, the sign of LNH is a useful indicator of the changes in the direction of the rotation of flow during the cardiac cycle. Taking advantage of the property of the density per unit volume of kinetic helicity (Eq. 2) to change sign across a separation or reattachment line (Moffatt and Tsinober 1992), an opposite sign of the local value of LNH allows a local right-handed or left-handed rotation to be identified.

If we consider the trajectory described by a generic particle labeled k moving in a vessel, using the flow descriptor LNH, its dynamics can be characterized by means of the following quantity:

$$hfi_k = \frac{1}{\left(\mathrm{T}_k^{end} - \mathrm{T}_k^{start}\right)} \int_{\mathrm{T}_k^{start}}^{\mathrm{T}_k^{end}} |\mathrm{LNH}_k\,(\varsigma)|\mathrm{d}\varsigma \quad 0 \leq hfi_k \leq 1, \tag{4}$$

which represents the integral sum, in time, of the LNH values experienced by the kth particle moving along its trajectory during the time interval $\left(\mathrm{T}_k^{end} - \mathrm{T}_k^{start}\right)$. For each particle set injection (see Fig. 2, lower panel), hfi_k values were calculated over a time interval $\left(\Delta\mathrm{T}_k = \mathrm{T}_k^{end} - \mathrm{T}_k^{start}\right)$ between the time of injection T_j and the end of systole T_{es}, or upon the time interval needed for particles to leave the fluid domain if the latter is shorter than systole (i.e., $\mathrm{T}_k^{end} < \mathrm{T}_{es}$).

Over the N_p particles moving in the fluid domain, the helical flow index can be calculated as

$$\mathrm{HFI} = \frac{1}{N_p}\sum_{k=1}^{N_p} hfi_k \quad 0 \leq \mathrm{HFI} \leq 1. \tag{5}$$

For each particle set injection (see Fig. 2, lower panel), hfi_k values were calculated on particle traces over the time interval $\Delta\mathrm{T}_k$.

Finally, the mean value of HFI calculated over particle sets emitted at the $\mathrm{N}_T = 5$ time points can be calculated:

$$\overline{\mathrm{HFI}} = \frac{1}{N_T}\sum_{j=1}^{N_T} \mathrm{HFI}_j \qquad 0 \leq \overline{\mathrm{HFI}} \leq 1. \tag{6}$$

Equation 6 is the expression, as an average, of the helical content within the streaming blood through the systolic phase.

2.5 Statistical analysis

An intra-individual statistical analysis was performed for the five aortas under investigation to clarify whether helical blood flow depends on the phase of the cardiac cycle.

For all subjects and for all of the investigated time points T_j for release of the particle sets, the values of hfi_k (Eq. 4)—the HFI computed along each kth particle trajectory over the time interval ΔT_k—were used to investigate differences in helical flow content in terms of the phase of systole. Statistical analyses (Matlab Statistical toolbox, The Mathworks, Natick, MA, USA) were performed by applying the non-parametric two-sample Kolmogorov–Smirnov test (Kolmogorov 1956). This test is sensitive to differences in both the location and shape of the empirical cumulative distribution functions of the two samples and does not need any basic hypotheses for the sample distributions. The Jarque–Bera test (Bera and Jarque 1981), which measures the departure from normality based on the sample kurtosis and skewness, was previously performed to verify the hypothesis of normal distribution for each one of the five individual jth subpopulation of hfi_k values. The critical significant level was set at $\alpha = 0.1$ (according to the guidelines for reporting statistics of the American Physiological Society, aimed at finding an effect that could lead to a promising scientific discovery). High-order standardized moments were also calculated to obtain a measure of possible differences in percent distributions of hfi_k values.

3 Results

This section is organized in three subsections. In the first subsection, map frames of the acquired PC MRI data and visualization of related velocity vector fields are provided. In the second subsection, we describe and compare both the intra-individual and the inter-individual complex blood flow evolution in the five aortas under investigation adopting a Lagrangian representation. Results reported in the third subsection will illustrate the effectiveness of the algorithm proposed for quantification of helical flow in relation to the investigated human aortas.

3.1 PC MRI data visualization

Figure 1, introduced in the "Materials and Methods" section, displays the map frames (that span mid-systole) of the measured three-directional velocity components (phase I, II, and III) for each of the healthy subjects under investigation, on a plane aligned with the aortic arch.

Notably, the out-of-plane velocity component (phase III) exhibits a clearly identifiable light strip against the inner wall of the upper arch during flow deceleration (T_5), with a broader dark region near the outer wall of the arch (dark away from viewer, light toward viewer). This finding is consistent with the existence of a rotational flow pattern as a feature common not only to all of the human aortas investigated herein but also to previous bidirectional (Kilner et al. 1993) and three-directional observations (Markl et al. 2004; Morbiducci et al. 2009a).

A more clear depiction of the temporal development of flow on a plane aligned with the aortic arch (the same as Fig. 1) is given in Fig. 3. The visualization of the velocity vector maps obtained by processing phase-contrast data highlights features common to the five subjects:

(1) High axial flow velocities first appear close to the inner curvature (Fig. 3, left and mid-panel, i.e., T_3 and T_4); the streaming blood close to the inner wall gains more speed as a consequence of the transient nature of blood flow in aorta, which partially inhibits the circulation of the velocities and mitigates its centrifugal effects.
(2) When axial flow declines in the second part of systole, a migration of the highest velocities outward can be observed in the arch, and a retrograde stream (Fig. 3, right panel, i.e., T_5) arises from the relatively slow blood flow close to the inner curvature.

An overall similarity of the data can be observed among the five subjects under investigation (Figs. 1, 3).

3.2 Lagrangian analysis: three-dimensional evolution of the aortic flow

Particle traces give both a synthetic spatial and temporal depiction of the features of unsteady flow fields. As an example, movie I displays the evolving flow patterns in the aorta of subject E, obtained by means of Lagrangian analysis, on the particle set emitted at peak systole and fused to the modulus image of the aorta (see Supplementary Data). Here, we use the definition of the pseudo-scalar quantity LNH (Eq. 3). Color-coding of the particle traces in terms of LNH can be used to display how helical structures in blood flow rotate; an instantaneous positive (negative) value of the LNH gives evidence of a right- (left-) handed rotation. Like that of a corkscrew, this helix is clockwise (counter clockwise) when viewed in the direction of forward movement.

From Lagrangian analysis, hemodynamic features emerged that are common to the healthy population under investigation.

The evolution of particle sets emitted during early systole highlights the fact that blood is conveyed into the

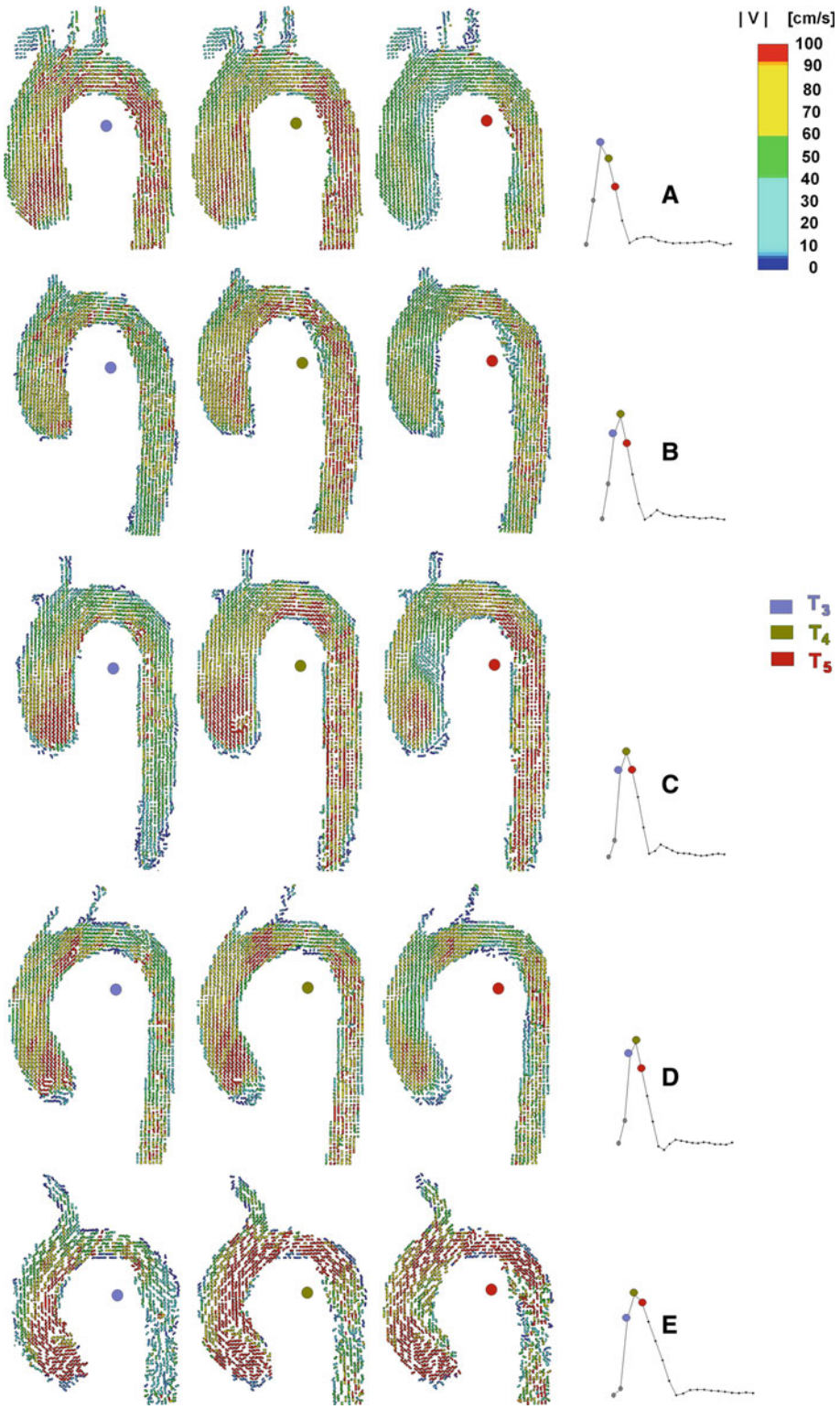

Fig. 3 Temporal development (T_3—yellow, T_4—green, and T_5—red) of flow depicted by velocity vector maps obtained by processing phase-contrast data on a plane aligned with the aortic arch. High axial flow velocities first appear close to the inner curvature (*left and mid-panels*). When axial flow declines (*right panel*), a migration of the highest velocities outward can be observed in the arch and a retrograde stream arises from relatively slow blood close to the inner curvature

aorta with streaming patterns aligned with the aortic axis; no formation of evident helical vortices developing in the ascending aorta and the proximal aortic arch can be appreciated (Fig. 4, visualization of particle sets emitted at T_2).

The visualization of traces of particle sets emitted at peak systole allows us to observe that helical patterns begin to emerge in the flow field of all of the subjects. In particular, helical structures with right-handed rotation begin to appear toward the inner wall and persist in the upper arch (Fig. 5);

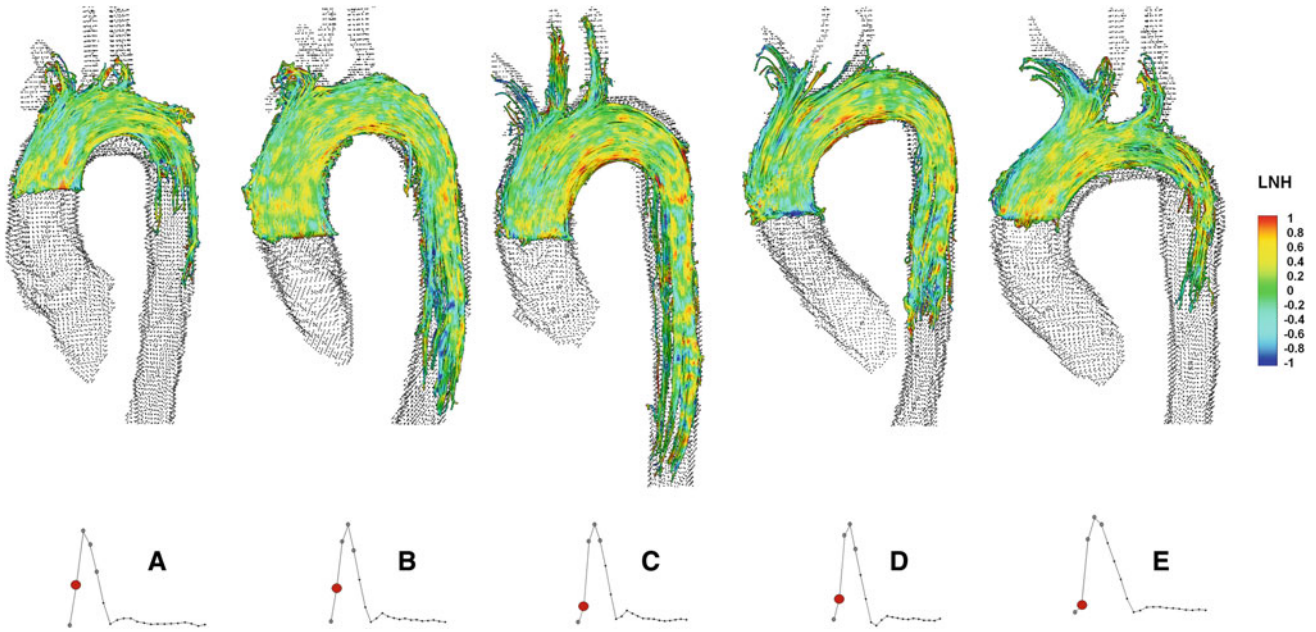

Fig. 4 Evolution of the particle sets emitted during the flow acceleration phase (T_2) fused to the three-dimensional shape of the aortas. Color-coding of the particle traces was used to display the instantaneous value of the LNH (*right-handed* positive value, *left-handed* negative value). In all of the subjects, no formation of evident helical vortices developing in the ascending aorta and the proximal aortic arch can be noticed. Blood streaming patterns are also aligned with the aortic axis in all of the subjects

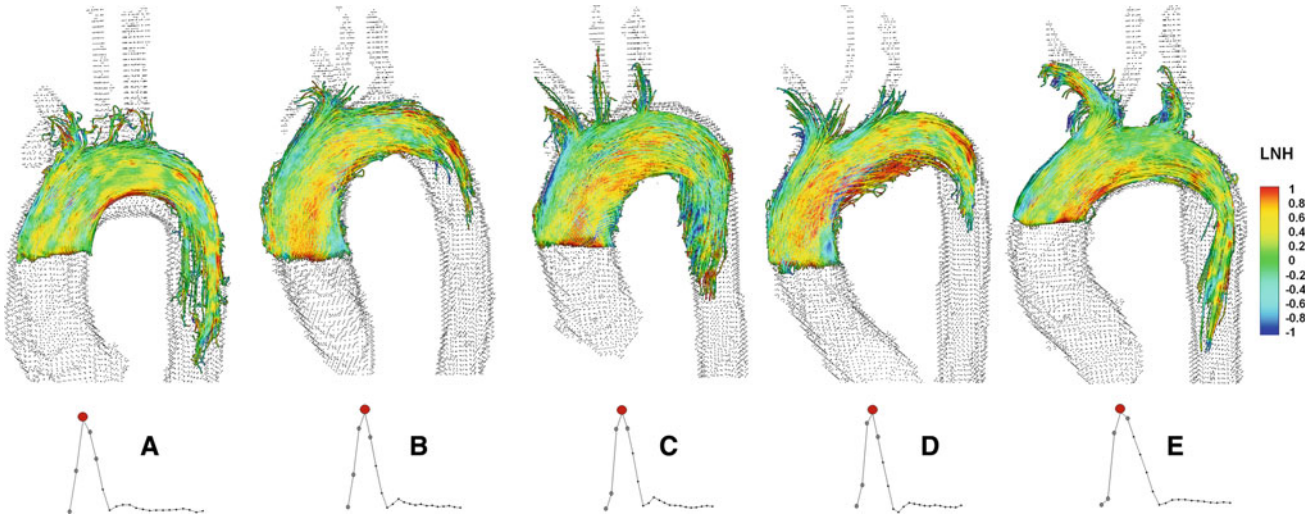

Fig. 5 Evolution of the particle sets emitted at peak systole, fused to the three-dimensional shape of the aortas. Color-coding of the particle traces was used to display the instantaneous value of the LNH (*right-handed* positive value, *left-handed* negative value). More coherent helical structures begin to emerge in the aortic flow. In all patients, the onset of *right-handed helical* structures at the inner wall of the aorta (from this view) is worth noting

additionally, left-handed rotation helices, which vanish in the mid-arch, are present toward the outer wall.

The analysis of the five datasets highlights the observation that the evolution of the particle set emitted after peak systole is strongly characterized by the onset of more coherent helical structures (Fig. 6). This behavior, which was present in all of the subjects under investigation, supports our hypothesis (Morbiducci et al. 2009a) that the helical arrangement of the flow at the inner curvature of the arch forms in an attempt to compensate for curling the forward streaming blood to fill the space left by the flow separation at the inner wall (see Figs. 1, 3).

The fluid rotational momentum dominates the flow deceleration phase, resulting in coherent helical and bi-helical pat-

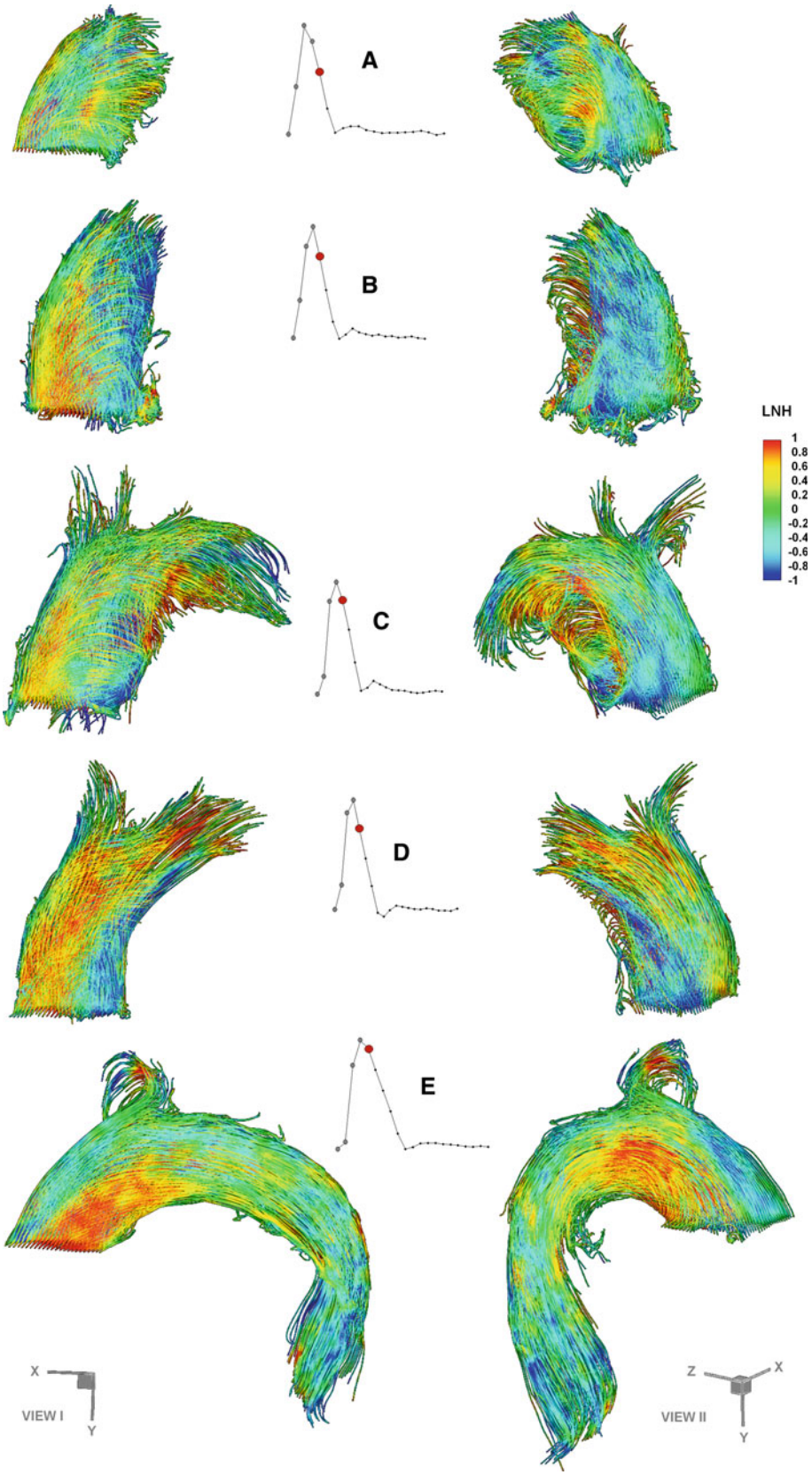

Fig. 6 Evolution (two different views) of the particle set emitted during the flow deceleration phase (T_5) in the five aortas under investigation. Color-coding of the particle traces was used to display the instantaneous value of the LNH. The topology of the flow begins to assume helical (subject **A**, **E**) and bi-helical structures (subject **B**, **C**, **D**), with an inversion in the helical rotation going from the inner (*right-handed* positive values of LNH) to the outer (*left-handed* negative values of LNH) aortic wall

terns in the ascending aorta. Particle traces relative to particle sets emitted after the peak of systole show that a coherent helical field characterizes blood flow topology in this phase of the cardiac cycle, with rotating or counter-rotating helical structures. This phenomenon is clearly visible in Fig. 6, which depicts the evolving flow for particle sets emitted at T_5.

In particular, the two different views displayed in Fig. 6 highlight that the topology of the flow begins to assume a single (subject A, E) or double (subject B, C, D) swirl-like structure, with an inversion in the helical rotation from the inner (right-handed, positive values of LNH) to the outer (left-handed, negative values of LNH) aortic wall.

The onset of helical patterns in the ascending plus proximal aorta in the second half of systole can be viewed in Fig. 7, which displays the first 25 ms of the dynamics of particle sets emitted at T_5. The image is oriented as if viewed from the aortic orifice.

The visualization demonstrates definitively that the composition of the rotating vortices and the axial flow results in the helical (subject A, E) and bi-helical (subject B, C, D) arrangement of the flow field in the ascending aorta and the proximal tract of the arch in late systole.

3.3 Helical flow quantitative analysis

Figure 8 summarizes the HFI values calculated over traces of particle sets emitted at the five time points T_j during systole (through the end of systole). Results from the analysis of all of the healthy individuals investigated herein are shown. In general, the following features are common to all of the subjects: (1) particle sets emitted after the systolic peak are characterized by the highest helical content; (2) particle sets emitted during the first phase of systole (T_1 through T_3) are characterized by similar trends in HFI values (with the sole exception of subject E for the particle set emitted at T_3); (3) on average, regarding the subjects investigated, the HFI value calculated for the particle set emitted at T_5, mid-late systole, is 27% (SD 13) higher than the HFI value calculated for the particle set emitted at T_1 at early systole.

For each subject under investigation, an intra-individual statistical analysis was carried out on particle sets emitted at phases T_j ($j = 1, \ldots, 5$) of the cardiac cycle and evolving into the aorta through systole. The following results were obtained.

(1) The Jarque–Bera test for goodness-of-fit to a normal distribution showed that the distributions of hfi_k values (Fig. 9) deviate from normality in almost all of the particle sets T_j. The hypothesis of normal distribution for the hfi_k values cannot be rejected only for subject C at emission T_4 ($P = 0.99$) and T_5 ($P = 0.54$), and for subject D at T_4 ($P = 0.44$). Notably, the hypothesis of normal distribution for the hfi_k values holds true only for particle sets emitted at mid-late systole.

(2) Significant differences among hfi_k values belonging to different particle sets were confirmed by the Kolmogorov–Smirnov test. We found that there are always significant statistical differences (see Fig. 9), except in the cases of subject A between particle sets emitted at T_4 and T_5 ($P = 0.49$) and subject D in particle sets emitted at T_1 and T_2 ($P = 0.44$). Notably, hfi_k distributions with no statistical difference belong to the same phase of the cardiac cycle (i.e., mid-late systole for subject A and early systole for subject D).

The results from statistical analysis, together with the individual HFI values (i.e., the mean of the hfi_k values of the particle set emitted at T_j) summarized in Fig. 8, enforce our recent supposition that the helical content strongly depends upon the evolution of the flow through the aorta (Morbiducci et al. 2009a).

Figure 10 displays the $\overline{\text{HFI}}$ values calculated over particle sets emitted at the five time points (summarized in Fig. 8).

Notably, the aortic hemodynamics of the healthy subjects investigated herein are characterized by very similar values of $\overline{\text{HFI}}$ (Fig. 10, lower panel), even if slight differences were observed.

4 Discussion

Real blood flow dynamics in the thoracic aorta is an intricate process that involves interaction, reconnection, and continuous re-organization of helical and vortical fluid structures. In 1996, important studies contributed to the discussions on the role played by helical flow patterns in arteries, stating that relatively coherent swirling of blood might avoid excessive dissipation of energy by limiting flow instability in arteries (Caro et al. 1996; Stonebridge et al. 1996). For this reason, analyzing and understanding energy transfer and dissipation in the aortic hemodynamics is of fundamental importance. However, the physiological significance of the features of aortic blood flow is still debated.

From theoretical fluid mechanics, we speculate that during the cardiac cycle the flow topology changes, altering the helicity of the system due to a local exchange of writhe and twist helicity in the interacting tube strands (Moffatt 1969). This is clearly a key mechanism to understanding energy dissipation in real fluids. However, thus far, very little work has been done to investigate these aspects in vivo in the human aorta. Consistent with the fundamental role recognized for helicity in the organization of both laminar and turbulent flows, we postulated that the onset of helical patterns in aortic hemodynamics could also be explained in terms of energy dissipation (Morbiducci et al. 2009a). The results of this

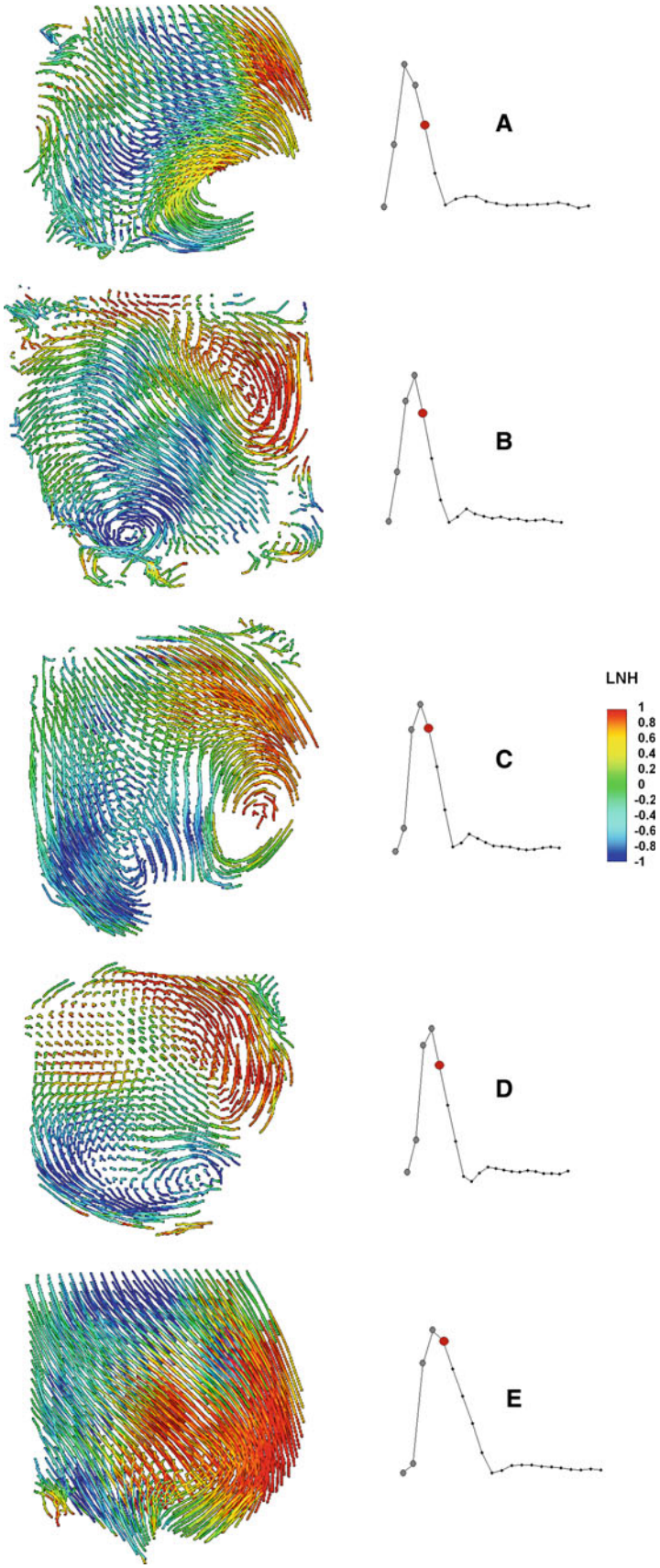

Fig. 7 First 25 ms of the dynamics of particle sets emitted during the flow deceleration phase (T_5) in the five aortas under investigation. The image is oriented as if the observer is looking from the bottom. Color-coding of the particle traces was used to display the instantaneous value of the LNH (*right-handed* positive value, *left-handed* negative value). The visualization unambiguously shows the presence of helical (subject **A**, **E**) and bi-helical (subject **B**, **C**, **D**) flow arrangement of the flow field in the ascending aorta and the proximal tract of the arch at late systole

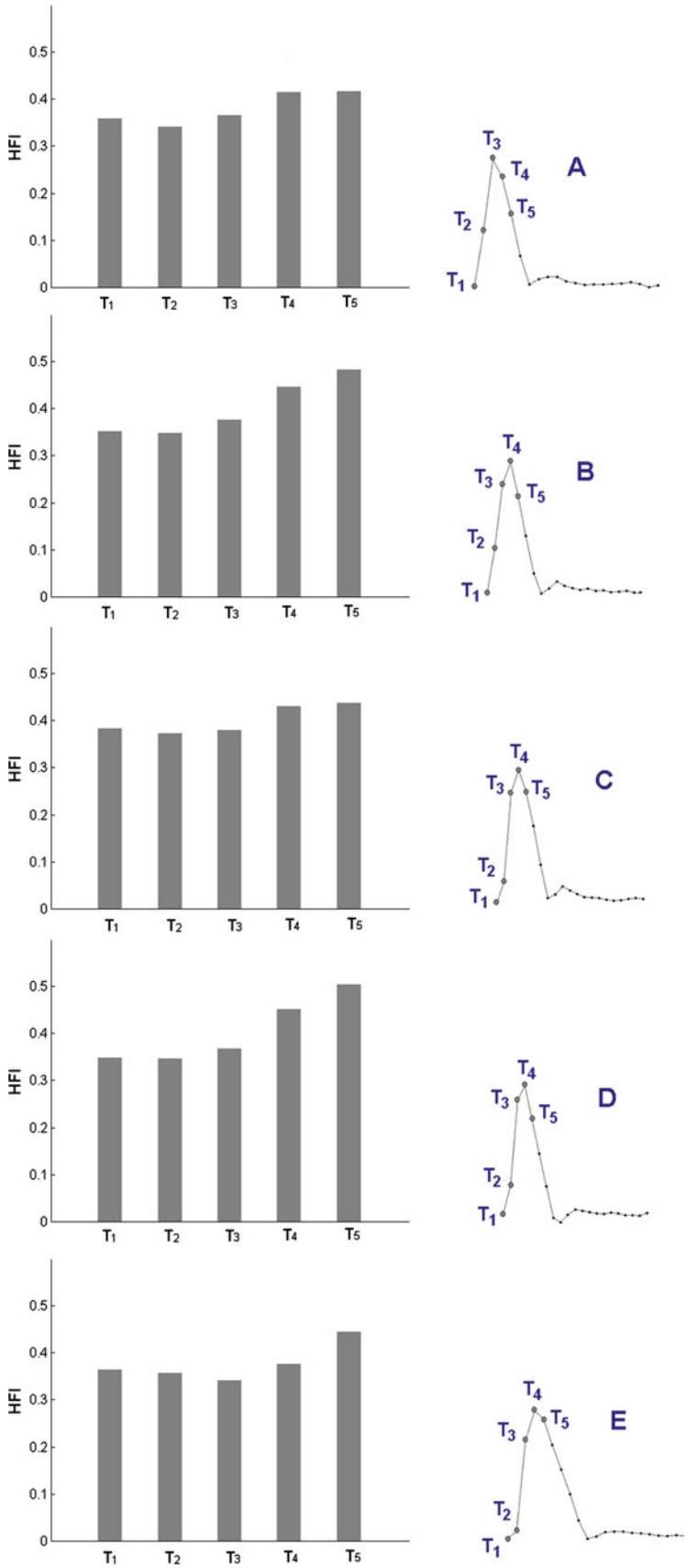

Fig. 8 HFI helicity indices calculated over traces of particle sets emitted at five time points, T_j, during systole (and over time intervals T_{es}–T_j). All of the subjects exhibit a similar trend in the HFI dynamics through systole

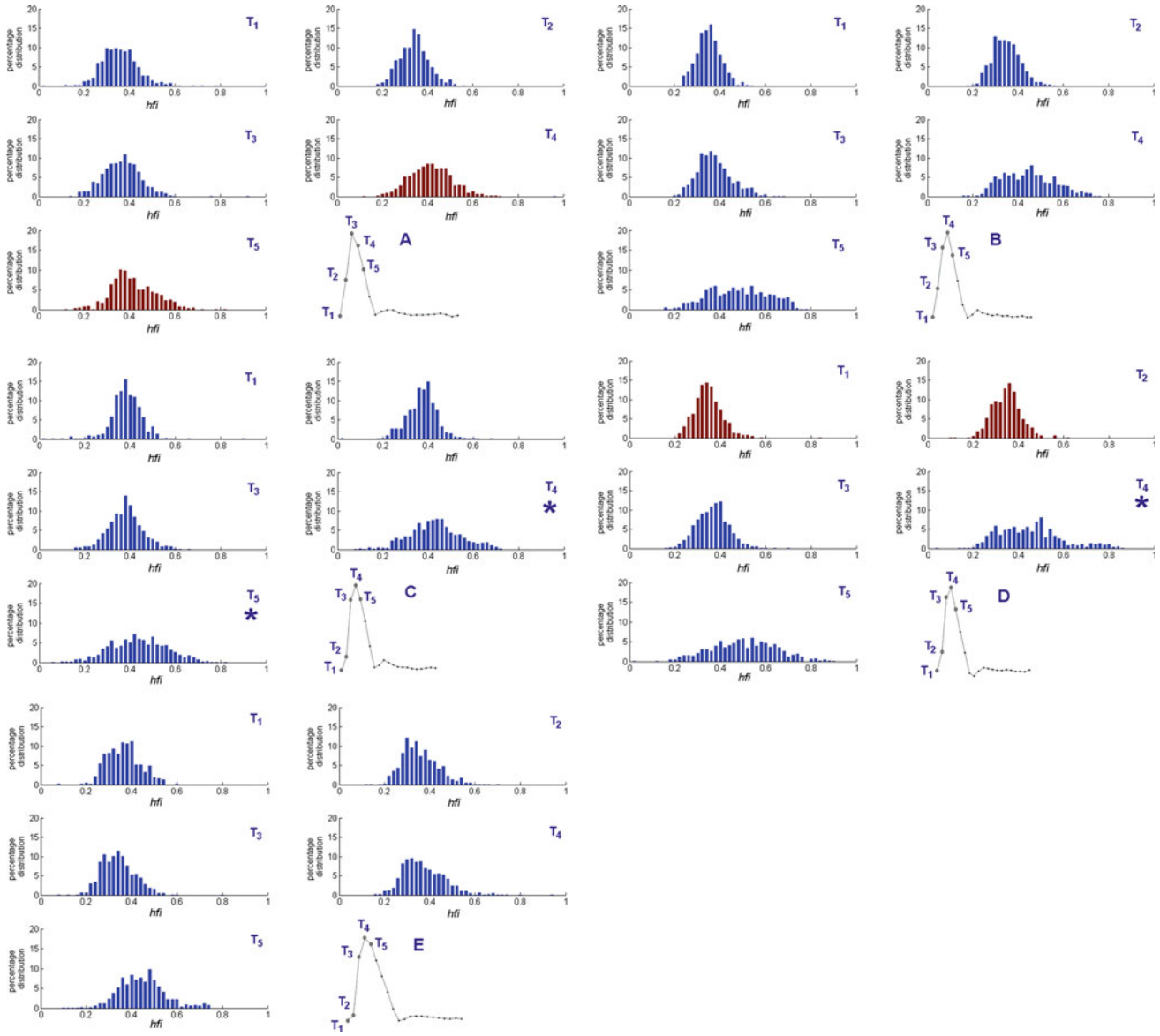

Fig. 9 Percent distribution of particle traces with respect to the helical flow index (*hfi*) computed along each particle trajectory. *Red bars* indicate *hfi* distributions that can be considered the same continuous distribution. They belong to the same phase of the cardiac cycle—mid-late systole for subject *A* and early systole for subject *D*. The hypothesis of normal distribution for the *hfi* values cannot be rejected for three * of the twenty-five cardiac phases analyzed (five for each subject)

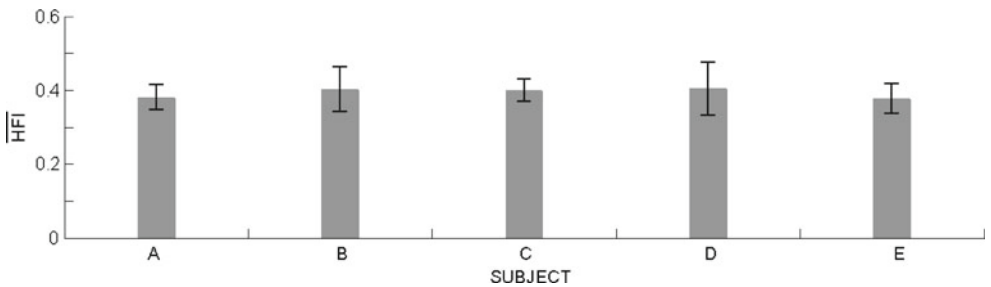

Fig. 10 $\overline{\text{HFI}}$ values calculated over particle sets emitted at five time points (see Fig. 8). Similar $\overline{\text{HFI}}$ values characterize the hemodynamics of the subjects investigated herein

study confirm and support this hypothesis; helicity formation might be the consequence of an optimization in naturally occurring fluid transport processes in the cardiovascular system, with the obtainment of an efficient perfusion as a result.

In particular, in the first half of the deceleration phase, when inertial effects determine the enhancement of the helical flow structures (as summarized in Figs. 6, 7), the action of transitional effects involves helicity to a significant extent. This feature works to mitigate loss of organization in the flow field and, as a consequence, transition to turbulence. Thus, the turbulent kinetic energy is reduced by the helical flow as it induces the rotational stability in the forward flow. This statement is enforced by the well-consolidated knowledge that many properties of systems presenting helicity are related to the reduction of non-linear processes responsible for the transfer and redistribution of energy through various scales. A non-zero helicity partially inhibits the energy flux from larger to smaller scales; helicity is expected to globally arrest the energy decay (Tsinober and Levich 1983; Moffatt and Tsinober 1992; Chen et al. 2003; Mininni et al. 2006; Teitelbaum and Mininni 2009). The extent to which non-zero helicity is expected to change Kolmogorov's law of energy decay rate ($-5/3$ slope for the energy decay) in anisotropic transitional viscous flows like blood depends upon specific cases that are beyond the scope of this work.

Hence, both theoretical considerations and our quantitative analysis suggest that the helicity in the aortic flow naturally develops to avoid excessive energy dissipation. In the process of conveying blood flow in the aorta (the site in the healthy circulatory system where the Reynolds number reaches the highest value), this characteristic has the beneficial consequence of contributing to minimize myocardial overloading.

The blood flow patterns in the five thoracic aortas show great similarity to previously reported measurements in healthy subjects (Kilner et al. 1993; Frazin et al. 1990; Bogren and Buonocore 1999; Wigström et al. 1999; Markl et al. 2004) and are enriched by quantitative evidence of helical patterns in the aorta:

(1) At early systole, no coherent helical patterns emerge from blood flow fields (Fig. 4);
(2) When the net forward flow is at a maximum, up to the end of systole, relatively coherent helical structures appear in the flow field, with the onset of helical structures located at the inner wall (Fig. 5);
(3) In the deceleration phase, when the weight of the inertial effects leads to a disorganization of the flow field, we found that the flow field topology in the ascending aorta and in the upper arch is characterized by high, more coherent helicity, associated with an onset of helical and bi-helical structures (Figs. 6, 7).

In recent years, several methods for characterizing flow structures have been successfully applied to cardiovascular flows. To quantify helical blood flow, a Lagrangian-based metric, the HFI, has been applied both in silico (Morbiducci et al. 2007a; Morbiducci et al. 2010) and in vivo (Morbiducci et al. 2009a). Moreover, the computation of Lagrangian coherent structures (Shadden and Taylor 2008; Shadden et al. 2010) and of another Lagrangian-based metric (Morbiducci et al. 2009b) has been demonstrated to be very useful to characterize (1) flow stagnation and separation, (2) partitioning of fluid to downstream vasculature, (3) vorticity dynamics, and (4) mechanisms governing stirring and mixing in both vascular models (Shadden and Taylor 2008) and in models of implanted prosthetic heart valves (Morbiducci et al. 2009b; Shadden et al. 2010). To the best of the authors' knowledge, only the HFI has been applied in vivo. This study confirms the strength of the helical flow index as a method for ranking the behavior of fluid dynamics within vessels in vivo and for giving a measurement of the structural complexity of flowing blood. While differences between flow patterns during the cardiac cycle, or between physiological and pathological cases, can be visually noted, an indicator or a metric-like HFI makes the level of comparison easier.

The intra-individual analysis highlights the finding that a general and statistically significant difference characterizes (Figs. 8, 9) the helical content of different phases of systole. A very similar behavior common to all of the subjects emerges from HFI-based quantitative analysis (Figs. 8, 10). This behavior offers a clear indication of the mechanistically driven dynamical arrangement of blood flow in helical patterns.

The fluid motion observed within these investigated human aortas shows inter-individual variability, which, in the opinion of the authors, could be ascribed to specific anatomical features (local subject-specific curvature/non-planarity of the ascending aorta), age, and heart rate of the subjects under investigation. In particular, the inter-individual velocity shifts and the non-synchronous arrangement in helical structures observed in the second half of systole could be ascribed to the different dynamics of the ventricular ejection among subjects and the different durations of their cardiac cycle. In fact, after visual inspection of Fig. 10, we noticed the following trends: (1) subjects B, C, and D, which exhibit very similar heart rate values (51 through 55 bpm), have comparable $\overline{\text{HFI}}$ values; (2) the hemodynamics of subjects A and E, which present heart rate of 43 and 78 bpm, respectively, are characterized by lower values of $\overline{\text{HFI}}$.

Hence, according to our preliminary findings, the scheme presented herein to assess helical blood flow in vivo could be helpful for answering important questions concerning circulation. As an example, this scheme could be applied to gain insight into the role played by hemodynamics in morphogenesis, where recent findings stated that the asymmetric devel-

opment of the aortic arch is governed by the establishment of hemodynamics determined by a genetically induced morphological change in the outflow tract of the heart (Yashiro et al. 2007).

For example, concerning the physiology of the aorta, the combined information given by the existence of a through-plane velocity component, which is clearly visible in Fig. 1 (as explained in the Results section) near the inner wall, joined with the velocity vector field evolution shown in Fig. 3, lead us to infer that the onset of helical flow could contribute to limiting flow separation at the inner curvature of the arch. This phenomenon also aids in enforcing the effect of flow circulation in transversal planes played by secondary flows, thus limiting/delaying the inversion of velocity at the inner wall. Moreover, this method could be used to investigate whether the basis of aortic helical physiological flow is in the ventricle fluid dynamics. Future studies could permit us to clarify to what extent the helicity in the aorta during early systole originates from the systolic ventricular function (Kilner et al. 2000; Gharib et al. 2006) and the role played by non-planarity in the main process of conveying blood in the axial direction in the aorta.

The proposed method for quantitative in vivo analysis could allow us also to gain knowledge concerning the nature of flow development in the arch and the presence of branches at the apex of the aortic arch. We could also investigate whether spiral flow patterns in the arteries may be more or less efficient in perfusing branch vessels (Stonebridge and Brophy 1991). This last aspect could also have great physiological relevance. In addition, it could be useful to evaluate the physiological significance of the aortic valve orifice shape, as HFI can quantify the swirling flow, recovering its critical features such as the slow-down of the axial speed near the center and the decay rate of the swirling strength.

We also believe that quantification of the helical content imposed by the heart on blood flow might allow detection of anomalies in the expected physiological development of helical flow. Accordingly, it could be used in diagnostics, prognostics, and therapeutics (Stonebridge and Brophy 1991; Hope et al. 2007; Markl et al. 2007; Frydrychowicz et al. 2008a,b; Weigang et al. 2008). In clinical practice, the use of a dimensionless index with the capability to both characterize and rank the flow motion (by assigning a score, for example) could be decisive when comparing patient groups; an analysis of hfi_k values similar to the one presented herein and depicted in Figs. 8 and 9 could become a useful instrument for discriminating among blood flow behaviors in the aorta.

The present study has limitations. Namely, we focused on normal subjects and our conclusions should not be extrapolated to the general population. A practical limitation of our study is that the number of subjects is relatively small in the context of large population studies. However, our results are consistent with many of the other studies reported in this manuscript, and we note that we are able to achieve statistical significance in many of the comparisons. Another limitation is that our study group does not include female subjects: sex dependence of helical flow dynamics will be the object of future investigations. We also did not explicitly assess the variability of measurements taken from the same subjects in repeated and non-consecutive sessions in separate scanning sessions that required subject repositioning. However, previous PC MRI studies suggest little or no difference between data acquired with or without repositioning of the subject (Spilt et al. 2002).

Even if simulations are beyond the scope of this paper, patient-specific modeling is the sole way to confirm questions of fluid mechanics raised in our study; the spatial and temporal resolution of state-of-the-art PC MRI scanners do not allow for reliable evaluations of turbulence through-scales transfer, dissipation, and/or decay. However, from a fluid mechanical standpoint, the theoretical relationships existing among quantities and parameters describing turbulence and helicity have not been confirmed by previous in vivo quantitative observations of cardiovascular flows. Consequently, in the future, we intend to take advantage of the potential of simulations and patient-specific modeling to calculate exact quantities, such as turbulence dissipation, and correlate them to helicity patterns.

Recently, in silico and in vitro studies (Grigioni et al. 2005; Fan et al. 2008; Morbiducci et al. 2007a; Morbiducci et al. 2007b; Sun et al. 2009; Liu et al. 2009; Zhan et al. 2010; Zheng et al. 2009) have vehemently renewed with quantitative results the presumption that the phenomenon of helicity in aortic hemodynamics also originates from the need for limiting flow instabilities in the vessels that could elicit fluid-wall interactions, leading to atherogenesis/atherosclerosis (Ku and Giddens 1983; Malek et al. 1999).

In the future, the Lagrangian-based determination of key downstream flow features could provide an efficient tool for ranking bulk blood flow in terms of its athero-susceptible/athero-protective potency. Recent studies support the hypothesis that a link exists between helicity and shear stress on the vascular wall. In particular, (1) Morbiducci et al. (Morbiducci et al. 2007a) demonstrated that the arrangement of the flow field in helical patterns in the aortocoronary bypass might elicit a damping in shear stress oscillations at the vessel wall, which is involved in flow-related arterial disease; (2) Chen and colleagues (Chen et al. 2009) found that intentional induction of helical flow in an endovascular stent reduced the size of the disturbed flow zones, enhanced the average wall shear stress, and lowered wall shear stress oscillations, which are adverse factors involved in the development of arterial restenosis after stent deployment; (3) the study by Liu et al. (28) assessed that the helical flow observed in the aorta may have great influence on the distribution of the luminal surface concentration of low density lipoproteins and, as

a consequence, on the spatial distribution of atheromatous plaques in the aorta.

Another important issue to be explored in the future is the incorporation of the metrics HFI and hfi_k in appropriate measures of performance for cardiovascular surgeries and interventions to be defined based on fluid mechanics information, as suggested by the recent developments in optimization methods applied to cardiovascular flows (Marsden et al. 2008). These metrics could also allow scientists to gain insight into the physiological/pathological development of helical flow in the aorta, both from in vivo data and from patient-specific numeric simulations.

Although the low number of subjects enrolled does not allow us to offer complete answers to questions pertaining to the origin and role played by helical blood flow in the human aorta, this study confirms that (1) the application of algorithms for the calculation of hemodynamics descriptors to 4D PC MRI datasets can make the in vivo quantification of helical blood flow possible (see Morbiducci et al. 2009a); (2) exploring the relationship between helical flow and hemodynamics is promising and makes the in vivo quantification of the helicity content very rewarding; (3) HFI has the potential for enriching aortic flow features common to healthy subjects with quantitative evidence and stands as a candidate metric to study the mechanistic relationships between physiological complexity and energy in the hemodynamics of the aorta.

Acknowledgments The Authors are sincerely thankful to Jill Diane Friedman for carefully reading the manuscript.

References

Amirbekian S, Long RC, Consolini MA, Suo J, Willett NJ, Fielden SW, Giddens DP, Taylor WR, Oshinski JN (2009) In vivo assessment of blood flow patterns in abdominal aorta of mice with MRI: implications for AAA localization. Am J Physiol Heart Circ Physiol 297:H1290–H1295

Baciewicz FA, Penney DG, Marinelli WA, Marinelli R (1991) Torsional ventricular motion and rotary blood flow. What is the clinical significance. Card Chron 5:1–8

Bellhouse BJ, Talbot L (1969) The fluid mechanics of the aortic valve. J Fluid Mech 35:721–736

Bera AK, Jarque CM (1981) Efficient tests for normality, homoscedasticity and serial independence of regression residuals: Monte Carlo evidence. Econ Lett 7(4):313–318

Bogren HG, Buonocore MH (1999) 4D magnetic resonance velocity mapping of blood flow patterns in the aorta in young vs. elderly normal subjects. J Magn Reson Imaging 10:861–869

Buonocore MH, Bogren HG (1999) Analysis of flow patterns using MRI. Int J Card Imaging 15:99–103

Caro CG, Doorly DJ, Tarnawski M, Scott KT, Long Q, Dumoulin CL (1996) Non-planar curvature and branching of arteries and non-planar-type flow. Proc R Soc Lond A 452:185–197

Chandran KB (1993) Flow dynamics in the human aorta. J Biomech Eng 115:611–616

Chen Q, Chen S, Eyink GL (2003) The joint cascade of energy and helicity in three-dimensional turbulence. Phys Fluids 15:361–374

Chen ZS, Fan YB, Deng XY, Xu Z (2009) Swirling flow can suppress flow disturbances in endovascular stents: a numerical study. ASAIO J 55(6):543–549

Darmofal DL, Haimes R (1996) An analysis of 3D particle path integration algorithms. J Comput Phys 123:182–195

David L, Esnault A, Calluaud D (2002) Comparison of techniques of interpolation for 2D and 3D velocimetry. In: Proceedings of the eleventh international symposium on applications of laser techniques to fluid mechanics, Lisbon

Fan Y, Xu Z, Jiang W, Deng X, Wang K, Sun A (2008) An S-type bypass can improve the hemodynamics in the bypassed arteries and suppress intimal hyperplasia along the host artery floor. J Biomech 41:2498–2505

Firmin D, Keegan J (2001) Navigator echoes in cardiac magnetic resonance. J Cardiovasc Magn Reson 3:183–193

Frazin LJ, Lanza G, Vonesh M, Khasho F, Spitzzeri C, McGee S, Mehlman D, Chandran KB, Talano J, McPherson D (1990) Functional chiral asymmetry in descending thoracic aorta. Circulation 82:1985–1994

Frydrychowicz A, Harloff A, Jung B, Zaitsev M, Weigang E, Bley TA, Langer M, Hennig J, Markl M (2007) Time-resolved, 3-dimensional magnetic resonance flow analysis at 3 T: visualization of normal and pathological aortic vascular haemodynamics. J Comput Assist Tomogr 31:9–15

Frydrychowicz A, Arnold R, Hirtler D, Schlensak C, Stalder AF, Hennig J, Langer M, Markl M (2008a) Multidirectional flow analysis by cardiovascular magnetic resonance in aneurysm development following repair of aortic coarctation. J Cardiovasc Magn Reson 10(1):30

Frydrychowicz A, Arnold R, Harloff A, Schlensak C, Hennig J, Langer M, Markl M (2008b) Images in cardiovascular medicine. In vivo dimensional flow connectivity mapping after extracardiac total cavopulmonary connection. Circulation 118:e16–e17

Gharib M, Rambod E, Kheradvar A, Sahn DJ, Dabiri JO (2006) Optimal vortex formation as an index of cardiac health. Proc Natl Acad Sci USA 103:6305–6308

Grigioni M, Daniele C, Morbiducci U, Del Gaudio C, D'Avenio G, Balducci A, Barbaro V (2005) A mathematical description of blood spiral flow in vessels: application to a numerical study of flow in arterial bending. J Biomech 38:1375–1386

Hope TA, Markl M, Wigström L, Alley MT, Miller DC, Herfkens RJ (2007) Comparison of flow patterns in ascending aortic aneurysms and volunteers using four-dimensional magnetic resonance velocity mapping. J Magn Reson Imaging 26:1471–1479

Houston JG, Gandy SJ, Sheppard DG, Dick JB, Belch JJ, Stonebridge PA (2003) Two-dimensional flow quantitative MRI of aortic arch blood flow patterns: Effect of age, sex, and presence of carotid atheromatous disease on prevalence of spiral blood flow. J Magn Reson Imaging 18:169–174

Kilner PJ, Yang GZ, Mohiaddin RH, Firmin DN, Longmore DB (1993) Helical and retrograde secondary flow patterns in the aortic arch studied by three-directional magnetic resonance velocity mapping. Circulation 88:2235–2247

Kilner PJ, Yang GZ, Wilkes AJ, Mohiaddin RH, Firmin DN, Yacoub MH (2000) Asymmetric redirection of flow through the heart. Nature 404:759–761

Kolmogorov AN (1956) Foundations of the theory of probability, 2nd English edn. Chelsea Publishing Company, New York (translation edited by Nathan Morrison)

Ku DN, Giddens DP (1983) Pulsatile flow in a model carotid bifurcation. Arteriosclerosis 3:31–39

Liu X, Pu F, Fan Y, Deng X, Li D, Li S (2009) A numerical study on the flow of blood and the transport of LDL in the human aorta:

the physiological significance of the helical flow in the aortic arch. Am J Physiol Heart Circ Physiol 297:H163–H170
Malek AM, Alper SL, Izumo S (1999) Hemodynamic shear stress and its role in atherosclerosis. JAMA 282:2035–2042
Markl M, Draney MT, Hope MD, Levin JM, Chan FP, Alley MT, Pelc NJ, Herfkens RJ (2004) Time-resolved 3-dimensional velocity mapping in the thoracic aorta: visualization of 3-directional blood flow patterns in healthy volunteers and patients. J Comput Assist Tomogr 28:459–468
Markl M, Harloff A, Föll D, Langer M, Hennig J, Frydrychowicz A (2007) Sclerotic aortic valve: flow-sensitive 4-dimensional magnetic resonance imaging reveals 3 distinct flow-pattern changes. Circulation 116:e336–e337
Marsden AL, Feinstein JA, Taylor CA (2008) A computational framework for derivative-free optimization of cardiovascular geometries. Comput Methods Appl Mech Eng 197:1890–1905
Mininni PD, Alexakis A, Pouquet A (2006) Large scale flow effects, energy transfer, and self-similarity on turbulence. Phys Rev E 74:016303
Moffatt HK (1969) The degree of knottedness of tangled vortex lines. J Fluid Mech 36:17–29
Moffatt HK (1990) The energy spectrum of knots and links. Nature 347:367–369
Moffatt HK, Tsinober A (1992) Helicity in laminar and turbulent flow. Ann Rev Fluid Mech 24:281–312
Morbiducci U, Ponzini R, Grigioni M, Redaelli A (2007a) Helical flow as fluid dynamic signature for atherogenesis in aortocoronary bypass. A numeric study. J Biomech 40:519–534
Morbiducci U, Lemma M, Ponzini R, Boi A, Bondavalli L, Antona C, Montevecchi FM, Redaelli A (2007b) Does flow dynamics of the magnetic vascular coupling for distal anastomosis in coronary artery bypass grafting contribute to the risk of graft failure. Int J Artif Organs 30:628–639
Morbiducci U, Ponzini R, Rizzo G, Cadioli M, Esposito A, De Cobelli F, Del Maschio A, Montevecchi FM, Redaelli A (2009a) In vivo quantification of helical blood flow in human aorta by time-resolved three-dimensional cine phase contrast MRI. Ann Biomed Eng 37:516–531
Morbiducci U, Ponzini R, Nobili M, Massai D, Montevecchi FM, Bluestein D, Redaelli A (2009b) Blood damage safety of prosthetic heart valves. Shear induced platelet activation and local flow dynamics: a fluid-structure interaction approach. J Biomech 42(12):1952–1960
Morbiducci U, Gallo D, Ponzini R, Massai D, Antiga L, Redaelli A, Montevecchi FM (2010) Quantitative analysis of bulk flow in image-based haemodynamic models of the carotid bifurcation: the influence of outflow conditions as test case. Ann Biomed Eng. doi:10.1007/s10439-010-0099-y
Ponzini R, Morbiducci U, Iannaccone F, Rizzo G, Cadioli M, Vismara R, Redaelli A (2009) Synthetic 4D phase contrast MRI datasets: a CFD-based approach for the validation of advanced fluid-dynamics calculations in vivo. In: Tavares JM, Natal Jorge RM (eds) Proceedings of VIPIMAGE 2009, Second Ecomas Thematic Conference on Computational Vision and Medical Image Processing, Porto. CRC Press, Taylor & Francis Group, pp 195–199
Ricca RL (2009) Structural complexity and dynamical systems. In: Ricca RL (ed) Lectures on topological fluid mechanics. Lecture notes in mathematics. Springer, Berlin, pp 167–186
Seed WA, Wood NB (1971) Velocity patterns in the aorta. Cardiovasc Res 5:319–330
Segadal L, Matre K (1987) Blood velocity distribution in the human ascending aorta. Circulation 76:90–100
Shadden SC, Taylor CA (2008) Characterization of coherent structures in the cardiovascular system. Ann Biomed Eng 36(7):1152–1162
Shadden SC, Astorino A, Gerbeau JF (2010) Computational analysis of an aortic valve jet with Lagrangian coherent structures. Chaos 20:017512
Spilt A, Box FM, van der Geest RJ, Reiber JH, Kunz P, Kamper AM, Blauw GJ, van Buchem MA (2002) Reproducibility of total cerebral blood flow measurements using phase contrast magnetic resonance imaging. J Magn Reson Imaging 16:1–5
Steinman DA (2000) Simulated pathline visualization of computed periodic blood flow patterns. J Biomech 33:623–628
Stonebridge PA, Brophy CM (1991) Spiral laminar flow in arteries. Lancet 338:1360–1361
Stonebridge PA, Hoskins PR, Allan PL, Belch JF (1996) Spiral laminar flow in vivo. Clin Sci (Lond) 91:17–21
Sun A, Fan Y, Deng X (2009) Numerical investigation of blood flow in the distal end of an axis-deviated arterial bypass model. Biorheology 46:83–92
Teitelbaum T, Mininni PD (2009) Effect of helicity and rotation on the free decay of turbulent flows. Phys Rev Lett 103:014501
Tsinober A, Levich E (1983) On the helical nature of three dimensional coherent structures in turbulent flows. Phys Lett 99:321–323
Weigang E, Kari FA, Beyersdorf F, Luehr M, Etz CD, Frydrychowicz A, Harloff A, Markl M (2008) Flow-sensitive four-dimensional magnetic resonance imaging: flow patterns in ascending aortic aneurysms. Eur J Cardiothorac Surg 34:11–16
Wigström L, Ebbers T, Fyrenius A, Karlsson M, Engvall J, Wranne B, Bolger AF (1999) Particle trace visualization of intracardiac flow using time-resolved 3D phase contrast MRI. Magn Reson Med 41:793–799
Yashiro K, Shiratori H, Hamada H (2007) Haemodynamics determined by a genetic programme govern asymmetric development of the aortic arch. Nature 450:285–288
Yearwood TL, Chandran KB (1982) Physiological pulsatile flow experiments in a model of the human aortic arch. J Biomech 15(9): 683–704
Zhan F, Fan Y, Deng X (2010) Swirling flow created in a glass tube suppressed platelet adhesion to the surface of the tube: its implication in the design of small-caliber arterial grafts. Thromb Res 125(5):413–418
Zheng T, Fan Y, Xiong Y, Jiang W, Deng X (2009) Hemodynamic performance study on small diameter helical grafts. ASAIO J 55:192–199